An Ultra-Compact Integrated Coherent Receiver for High Linearity RF Photonic Links

Uppiliappan Krishnamachari, Sasa Ristic, Anand Ramaswamy, Leif A. Johansson, Chin-Hui Chen, Jonathan Klamkin, Molly Piels, Ashish Bhardwaj, Mark Rodwell, John E. Bowers, Larry Coldren

Electrical and Computer Engineering Department
University of California, Santa Barbara
Santa Barbara, U.S.A

ukrishna@ece.ucsb.edu

***Abstract*—We demonstrate a novel photonic integrated circuit(PIC) that combines an ultra compact trench beam splitter with monolithically integrated detectors and modulators. A coherent receiver is realized by flip chip bonding of this PIC with an electronic integrated circuit(EIC). Preliminary system results yield an IMD3 distortion suppression of 46dB at a signal frequency of 300MHz.**

I. INTRODUCTION

Analog optical links are commonly used in the transmission of signals from antennas and electrical sensors from remote locations. Since these links are designed to convey low level signals from the antenna, high linearity and low-noise operation is required to retain the fidelity of the the input signal as closely as possible. The emphasis of this work is on the receiver end of the link which currently poses the greatest challenge in terms of system linearity requirements [1].

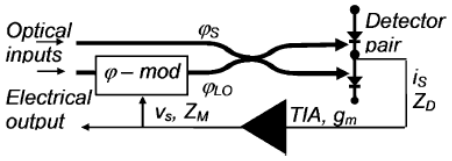

Fig. 1. Schematic outline of receiver architecture.

Linearity of analog optical receivers is limited in part by higher-order harmonic distortions of the RF signal. Due to system nonlinearities, spurious intermodulation products are created that mask or mimic real signals [2]. The third order intermodulation distortion(IMD3) is of particular concern because it falls within the useful bandwidth of the system. The figure of merit used to quantify the impact of the IMD3 on the system linearity is the spurious-free dynamic range(SFDR), and is defined as the ratio of the largest signal the system can transport to the smallest. Nonlinear distortion limits the maximum signal power and noise limits the minimum detectable signal power, comprising the upper and lower bounds of the dynamic range, respectively [3].

In traditional interferometer-based intensity modulated direct detection(IMDD) photonic links, the dominant limitation on dynamic range is the relative intensity noise, which is proportional to the square of the average optical power [4]. Furthermore, the modulation depth of MZM-based IMDD systems is limited to a range of 0-100%. In contrast, coherent phase modulated(PM) optical links are able to approach shot noise limited performance and the modulation depth can be much greater than 100%. Increasing the optical modulation depth leads to higher signal to noise ratio(SNR) and therefore higher dynamic range.

Another limit of overall link dynamic range is that any interferometer based receiver will have a sinusoidal response that will cause inherent nonlinearity, diminishing the benefits mentioned above. To overcome this limitation, we have previously proposed a coherent optical receiver that utilizes a reference tracking modulator with feedback [5]. The receiver architecture, shown in Fig. 1, consists of two phase modulators in push-pull configuration, two photodetectors in balanced configuration, a coupler for mixing the incoming signal with a local oscillator(LO) signal, and an electronic transconductance amplifier circuit. The local oscillator signal is split into two common paths each with a phase modulator. The input signal is applied to the first modulator, recombined with the LO in the coupler, and detected. The balanced PD produces an error signal which is amplified and fed back to the second phase modulator to compensate the phase difference between the signal and local oscillator. This effectively reduces the signal swing of the demodulator thereby restricting the operation of the receiver to the linear region of the response curve.

II. DEVICE DESIGN AND FABRICATION

In the first iteration of the coherent optical receiver, 2x2 multimode interference (MMI) couplers are used as the mixing element [6].

This material is based upon work supported by the DARPA-PHOR-FRONT program under United States Air Force contract number FA8750-05-C-0265

Use of a balanced detector suppresses the common mode relative intensity noise as well as amplifier noise [find ref]. UTC-PDs are employed for the balanced PDs because of their high photocurrent operation made possible by reduced space charge effects [7]. Push pull drive to symmetric tracking phase modulators is used to cancel even higher-order IMD terms[8]. To realize a large loop bandwidth, the capacitances of photodiodes and modulators are exploited as circuit elements to perform the desired loop integrations in the feedback path [9]. Because of bandwidth limitation due to latency in the loop, the delay must be kept short for stable operation at high frequency. Monolithic integration of the receiver components is necessary to limit the loop delay and maximize the optical power coupled to the PDs by avoiding additional coupling loss through unintegrated components. In [6], the PIC was wirebonded to an external EIC that provides transconductance amplification of the feedback signal. In the present iteration, we aim to reduce the loop delay of the original design by utilizing an ultra compact trench beam splitter to reduce the footprint of the PIC. This condensed design allows us to flip chip bond the EIC to the PIC, thereby substantially avoiding the delay of the wirebonds.

The monolithic integration platform for the coherent receiver is realized on semi-insulating InP substrate and requires a single regrowth step to form modulator and photodetector regions. The epitaxial structure, shown in Fig. 2, consists of the UTC-PD structure grown on top of unintentionally doped(UID) InGaAsP modulator QWs and barriers [11]. Photodetection regions are formed by selectively removing the UTC-PD layers, followed by a p-cladding and p-contact regrowth.

The optical waveguide uses a dry-etched deep ridge architecture to allow the flexibility of device geometry that the trench coupler requires. Comparatively, in surface ridge architectures, any features oriented significantly off the major plane suffer severe crystallographic undercut in the wet-etching process [12].

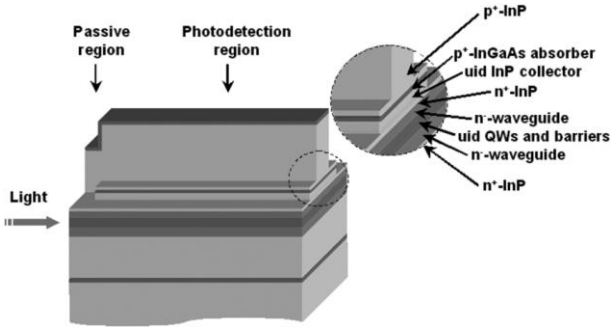

Figure 2. Device Epitaxial Structure

Waveguides are defined using a dual mask of 55nm Cr and 500nm SiO_2, and are deeply etched using Cl_2:H_2:Ar chemistry in an ICP system. Very low passive waveguide loss of 2.2 cm^{-1} has been reported for this deep etching process [13]. Next, mesas are etched, the InGaAs p+ contact layer is selectively removed between contacts to provide electrical isolation, and n- and p-contacts are deposited and annealed. In order to minimize diode series resistance, we first deposit a pre-metal layer which is a very thin stack of Pt/Ti/Pt/Au. This liftoff is carried out in such a way that the top p-side contact layer is not exposed until just before the metal deposition. This method largely avoids contamination of the metal- semiconductor interface, which is the most important factor in achieving low diode resistance.

Modulators of 500um length are defined in the metal deposition steps. The passive portions of the waveguide are proton implanted to drive down loss. To realize the balanced PD configuration, a series of high energy implants ranging from 40keV to 1.275 MeV are used to electrically isolate the n-contact layer. Transmission line model(TLM) measurements yield a sheet resistance of 4.8MΩ/square on the n-material and 1.9 MΩ/square on the p-material. The PDs are then able to be connected in series with minimal electrical cross talk between the diodes.

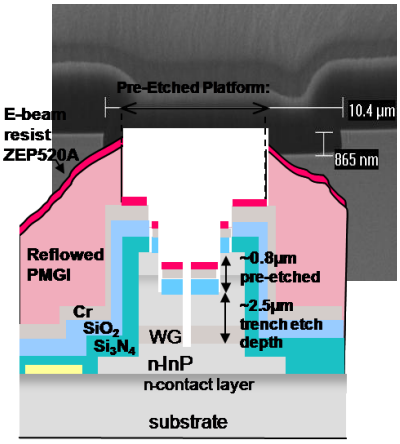

Figure 3(a) Trench coupler planarization process. (b) Cross-sectional SEM of pre-etched, BCB-filled trench coupler.

The trench coupler is designed to act as a frustrated total internal reflection(FTIR) mirror, reflecting and transmitting equal parts to the photodetectors. The input waveguide is incident on the FTIR mirror at an angle greater than the critical angle. Normally this should result in a fully reflected wave, but designing a narrow enough trench allows evanescent coupling of the incident wave across the trench that can result in an ultra compact 50/50 beam splitter. Benzocyclobutene(BCB) with a refractive index of 1.57 is used to fill in the trench. With a

calculated effective index of 3.265 for the waveguide, the critical angle is 28.5^{o}. Crossing angles in the range of 27^{0}-32^{0} were fabricated, correlating to trench widths of 0.25-0.5um. Trenches were written using electron beam lithography(EBL). Because ZEP-520 e-beam resist is very thin(~3000A), the topography of the sample, which has waveguides of over 3um height, makes it very challenging to get the necessary step coverage to provide a robust trench etch mask. Furthermore, the minimum thickness of the SiO_2 dielectric mask is 6000A, which is far too much to be etched using the thin e-beam resist. Therefore, a planarization process, using Polymethylglutarimide(PMGI) resist is employed. By reflowing the PMGI at 275^{0}C for 20min, the step height is reduced from 3.1um to 1.2um, which is within the step coverage tolerance of the e-beam resist. In order to reduce the required etch depth to reach the waveguide, a wider region around the trench is pre-etched down by ~1um. Simulations show that the effective index of the waveguide changes very little as a result of this pre-etching. This reduces the target etch depth to about 2um which is possible for the designed trench widths. A diagram of the pre-etching, planarization, and subsequent trench etch processes is shown in Fig. 3(a). A dual layer mask of Cr/SiO_2 is used as the trench hard mask. Both the pre-etch and the trench etch itself utilize the Cl_2:H_2:Ar chemistry used for the waveguide etch. Gas flows, pressure, and ICP power were varied to optimize the trench for depth, sidewall straightness and smoothness, resulting in a high aspect-ratio, low-loss trench coupler. A cross-sectional SEM of the optimized trench etch is shown in Fig. 3(b). After the trench etch, thick pad metal is deposited using an angled, rotating stage to ensure step coverage of the metal. A top view of the completed PIC is shown in Fig. 4(a)

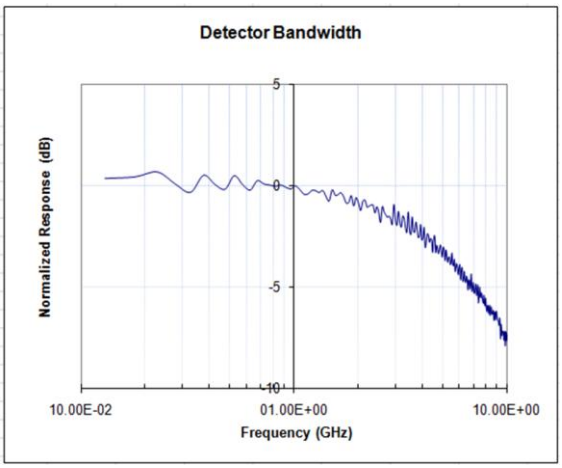

The last step of device fabrication is the integration of the transconductance amplifier EIC to the coherent receiver PIC by flip-chip bonding. After thick pad metal is deposited for the contacts, flip chip vias are opened and 2um tall Indium bumps are deposited to provide the contact points between the diodes of the PIC and the EIC connections. The PIC and the EIC are carefully aligned and bonded at a force of 1000g and a temperature of 200^{0}C. An SEM of the final integrated coherent receiver is shown in Fig. 4(b).

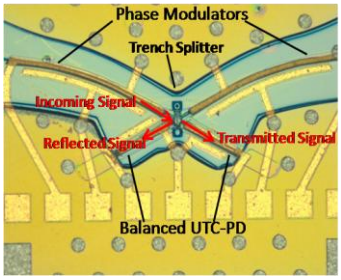

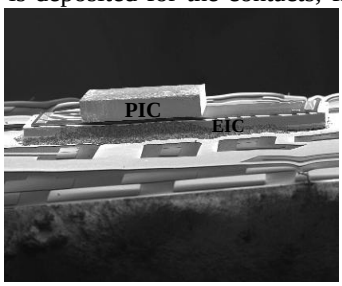

Figure 4(a) Top view of completed PIC. (b) Flip chip bonded PIC + EIC.

III. Integrated Receiver Results

The components of the integrated receiver are designed to achieve high power handling, high efficiency, and high linearity. Additionally, the architecture should be as compact as possible to minimize the overall loop delay. The total delay includes the delay incurred by the PIC, the EIC and the interconnections between them. In the MMI-based device reported in [6], the total loop delay is ~35ps, with a significant portion of the delay caused by the wirebond interconnects. In comparison, the ultra-compact trench-based flip chip bonded approach used in this work reduces the loop delay to ~10ps. This is expected to increase the open loop gain by 20dB at 1GHz, the target frequency of operation[Anands paper].

Diode performance was very good, presumably due to the pre-metal deposition process designed to avoid contamination of the metal-semiconductor interface. Measured diode resistance was ~5Ω for 300um x 3um modulators and ~20Ω for 50um x 7um detectors. Leakage currents were extremely low, typically in the nA range even for high reverse bias. Using a test electronic chip with direct traces to each diode contact, the PIC diode characteristics were measured before and after flip chip bonding. In most cases, the diode series resistance improved after flip chip bonding, perhaps because the In bumps make more stable contact than the pin probe used to test the diodes prior to bonding.

The efficiency and loss were measured for the phase modulators. For a 500um modulator, the V_{π} was measured to be 3.9V. The loss incurred between 0 V and V_{π} was 5.5 dB and the insertion loss was 1.04 dB. In Fig.5, the normalized PD response shows a 3dB bandwidth of ~5GHz for a 7um x150um device at -4V bias. This bandwidth is more than satisfactory for our link experiments carried out at 300MHz. Saturation and linearity measurements of the UTC-PDs were reported in [6]. Saturation current, defined as the photocurrent level where the RF

response is compressed by 1 dB, is reported to be 80mA at a bias of -3V. The third order output intercept point(OIP3), which is a measure of PD linearity, was found to be 46dBm at 60mA of DC photocurrent. The high performance of these UTC-PDs means that we can achieve high open loop gain without creating nonlinearities.

The trench coupler splitting ratio was tested under illumination from a laser source emitting at 1565nm. Light was fiber coupled into a phase modulator, split into reflected and transmitted waves at the trench, and detected at the UTC-PDs. A polarization controller was utilized to characterize the trench coupler for both TE and TM polarizations. By slightly reverse biasing the input phase modulator, we are able to select polarization by optimizing the modulator photocurrent. This is because transitions between the conduction and heavy hole bands in compressively strained quantum wells provide high TE absorption and low TM absorption [13]. Tuning the polarization to maximize the input phase modulator current selects TE polarized light, and minimizing selects TM polarized light. The maximum power transmitted through the trench occurs for TE polarized light, which also corresponds to the optimized splitting ratio for these devices. Several trench designs exhibited a TE splitting ratio very close to 50/50, with about 1.2mA into each detector at an input power of 10dBm. The detected TM photocurrent for the same device was 2mA and 0.4mA for the reflected and transmitted waves, respectively.

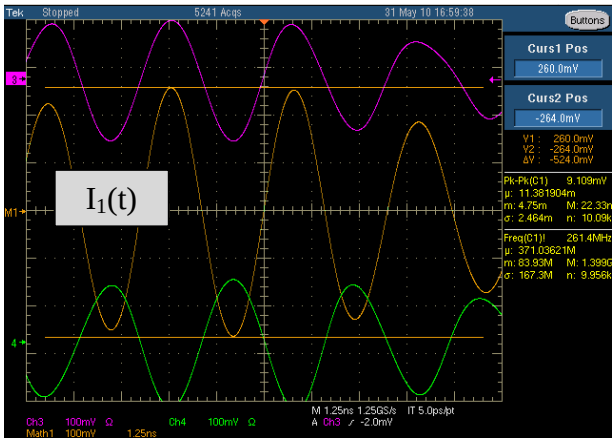

In order to get a measure of the trench coupler's mixing, we need to have input from both phase modulators simultaneously, reflecting and transmitting a mixed signal to each photodetector. To characterize this coherent mixing, we send a local oscillator signal to both phase modulator inputs and apply phase modulation to one arm. Following the derivation in [14], we assume a perfect 3dB coupler and detectors with the same responsivity, R. The detector photocurrents are given by:

The signal in the photodetectors will thus swing as the two input signals drift in and out of phase with each other. If we subtract the signals of the series connected photodetectors, we see the balanced detector output:

$$\Delta I(t) = I_1(t) - I_2(t) = 2R\sqrt{P_S(t)P_{LO}(t)} \cdot \sin\left((\omega_s - \omega_{LO}) \cdot t + \emptyset_s(t) - \emptyset_{LO}(t)\right)$$

Making the assumption that $P_S = P_{LO}$, (3) simplifies to:

$$\Delta I(t) = 2RP(t) \cdot \sin\left((\omega_s - \omega_{LO}) \cdot t + \emptyset_s(t) - \emptyset_{LO}(t)\right)$$

In ideal balanced detection, the balanced detector signal, $\Delta I(t)$ is swung through the full range of the sine function. The envelope of this balanced detector is the range from constructive to destructive interference of the input signals. Equation (4) simplifies to:

$$\Delta I_{p-p} = \Delta I_{max} - \Delta I_{min} = 2RP - (-2RP) = 4RP = 4\,I_{DC}$$

Therefore, in perfect balanced detection, the maximum amount of coherent mixing corresponds to a balanced detector signal swing of 4 x (average photocurrent in each detector). An oscilloscope trace of the balanced detector signal is shown in Fig. 5. The voltage swing of the individual photodetector signals, $V_1(t)$ and $V_2(t)$ are shown in the top and bottom traces. The middle trace is V_1-V_2, the balanced photodetector signal. Fiber coupling, polarization, and the relative power in each arm were optimized to find the maximum coherent mixing envelope. The oscilloscope has an input impedence of 50Ω. This means that the maximum voltage swing on the oscilloscope for perfect balanced detection is:

$$\Delta V_{p-p} = 50\Omega \cdot 4\,I_{DC}$$

The maximum observed signal swing for the device tested in Fig. 5 was found to be 524mV with an average I_{DC} of 3.5mA into each detector. The maximum possible signal swing is 700mV. Thus the coherence efficiency of the mixer is ~75%.

Having confirmed that the trench coupler coherently mixes the two incoming signals, we can then input the balanced detector signal to the transconductance amplifier feedback system to suppress receiver non-linearity. Preliminary two-tone measurements were carried out at signal frequencies of 298MHz and 300MHz(ask anand). Output frequency spectra of open loop vs. closed loop

operation of the integrated receiver are shown in Fig. 6. The input power was x dB per tone(ask anand). The IMD3 term is suppressed by an additional 46dB when the feedback loop is in operation, showing that the system does indeed suppress receiver nonlinearity. Assuming a shot-noise limited laser source, the calculated SFDR would be 122 dB·Hz$^{2/3}$. For detailed discussion of systems testing, see (anand's paper).

It should be mentioned that these systems results are far from optimized. The splitting ratio of the coherent receiver tested in Fig. 6 was roughly 20:80, far from the 3dB splitting that is optimal for coherent mixing. Furthermore, the facets of the tested device were not AR coated, which will drive down coupling efficiency and limit the input power because of the risk of burning the facet. Further, several EIC variants were fabricated. We believe that if we can achieve higher detector photocurrent, close to 50:50 splitting ratio, and pair this PIC with an optimized EIC variant, that we can achieve even higher dynamic range.

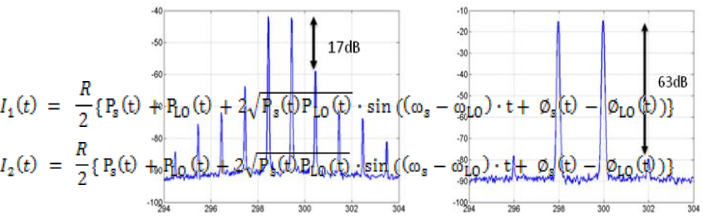

IV. CONCLUSION

Design and fabrication of a novel coherent receiver with feedback was presented. Flip chip bonding of the PIC to the EIC was used to reduce feedback latency. Trench beam splitters were developed to enable an ultra-compact PIC. We have achieved a very low latency of 10ps. Suppression of IMD3 by 46dBs was achieved. In future work, matching of PICs containing 50:50 beam splitters with the right EIC variant should enable further improvement in dynamic range.

REFERENCES

[1] 1.Coherent Receiver Based on a Broadband Optical Phase-Lock Loop, Ramaswamy)

[2] Dynamic Range of Coherent Analog Fiber-optic Links

[3] C. H. Cox, III, *Analog Optical Links Theory and Practice*. Cambridge, U.K.: Cambridge Univ. Press, 2004.).

[4] Characterization of a Balanced Modulation and Detection Analog Optical Link.

[5] SFDR Improvement of a Coherent Receiver Using Feedback," H.-F. Chou .

[6] Highly Linear Integrated Coherent Receivers for Microwave Photonic Links.

[7] T. Ishibashi, T. Furuta, H. Fushimi, S. Kodama, H. Ito, T. Nagatsuma, N. Shimizu, Y. Miyamoto, "InP/InGaAs Uni-Traveling-Carrier Photodiodes," *IEICE Trans. Electron.*, vol. E83-C, pp. 938-949, June 2000.

[8] Integrated Coherent Receivers for High-Linearity Microwave Photonic Links

[9] "Monolithically Integrated Coherent Receiver for Highly Linear Microwave Photonic Links," J. Klamkin).

[10] High Output Saturation and High-Linearity Uni-Traveling-Carrier Waveguide Photodiodes

[11] Selective Undercut Etching of InGaAs and InGaAsP Quantum Wells for Improved Performance of Long-Wavelength Optoelectronic Devices

[12] PROGRAMMABLE PHOTONIC FILTERS FABRICATED WITH DEEPLY ETCHED WAVEGUIDES

[13] **1.5 pm MQW semiconductor optical amplifier with tensile and compressively strained wells for polarizat ion-independent gain**

[14] Performance of balanced detection in a coherent receiver